FATIGUE ESTIMATION ON A HIGH-SPEED WAVE PIERCING CATAMARAN DURING NORMAL OPERATIONS

Reference NO. IJME736, DOI No: 10.5750/ijme.v164i1.736

M F Warren, **J Ali-Lavroff**, University of Tasmania, Australia, **J McVicar**, Revolution Design (Incat), Australia, **T Magoga,** Defence Science and Technology Group, Australia, **B Shabani,** University of Tasmania, Australia, **D S Holloway,** University of Tasmania, Australia, **G Thomas**, University College London, United Kingdom.

KEY DATES: Submitted: 04/06/21; Final acceptance: 25/04/22; Published 15/06/22

SUMMARY

The estimation of fatigue life in the design process is particularly important for weight-optimised ships such as high-speed aluminium craft, but to date no research has been published on the fatigue accumulation on large wave-piercing catamarans, focusing on long-term operations. This paper assesses the applicability of classification society rules for high-speed catamarans with respect to fatigue design. This was achieved by comparing the long-term distributions of stress, measured on a 111m long wave-piercing catamaran ferry whilst operating in the Canary Islands and during the delivery voyage, with load spectra estimated using a method accepted by the classification society, DNV. The paper also proposes an improved distribution fitment method for fatigue analysis. A detailed method to convert measured stress histories in the time domain into an appropriate stress-spectrum and fitment of Weibull parameters is presented. Results show that the simplified method accepted by the classification society is highly conservative regarding fatigue estimation compared to fatigue results based on measured data. The proposed combined Weibull fitment method substantially improves the accuracy of simplified fatigue analysis methods.

KEYWORDS

Fatigue, classification society, wave piercing catamaran, Weibull statistics

NOMENCLATURE

a_2	3 Parameter Weibull scale parameter (Equation 9)
D	Damage
E	Young's Modulus (Pa)
$F(\Delta\sigma_i)$	Cumulative Density Function
$f_s(\Delta\sigma_i)$	Probability Density Function
j	Number of stress amplitude bins
K	Stress concentration factor
k	2 Parameter Weibull shape parameter (Equation 10)
$\log_{10} a$	Fatigue parameter 1
m	Fatigue parameter 2
N_i	Number of cycles to failure at stress range i
N_{cycles}	Number of stress cycles kept after ranked cycle removal
n_i	Number of cycles at bin i
n_l	Number of cycles being analysed
$Q(\Delta\sigma_i)$	Exceedance Function
R^2	Coefficient of Determination
R_{range}	Ratio of maximum stress range to maximum stress
SD	Standard deviation
T_z	Assumed average ship response period (s)
$t_{section}$	Length of stress time-history (s)
w	2 Parameter Weibull scale parameter (Equation 10)
X	3 Parameter Weibull shape parameter (Equation 9)
Γ	Gamma function
$\Delta\varepsilon_0$	Maximum design strain range
$\Delta\sigma$	Stress Range (MPa)
$\Delta\sigma_0$	Design maximum stress range (MPa)
$\Delta\sigma_i$	Stress range at bin i (MPa)
δ	Coefficient of variation
λ	3 Parameter Weibull scale parameter (Equation 9)
μ_S	Mean stress (MPa)
σ_0	Design maximum stress (MPa)
$\sigma_{nominal}$	Nominal stress (MPa)
σ_{notch}	Notch stress (MPa)

1. INTRODUCTION

Wave Piercing Catamarans (WPCs) and more generally High-Speed Light Craft (HSLC) fulfil a requirement for fast and efficient transportation. This vessel type has been developed over the last 40 years to meet the needs of both commercial and military uses. The primary material of choice for the hulls of these vessels is marine-grade aluminium alloy due to its resistance to corrosion, low life-cycle costs, and high strength to weight ratio.

Incat Tasmania has been manufacturing high-speed, aluminium catamaran ferries, in Hobart, Tasmania since 1972 with design activities conducted by Revolution Design. These vessels have steadily increased in size and

complexity, the largest being 112.6m with a maximum speed of approximately 40 knots (INCAT, 2019). Other shipbuilders in Australia such as Austal Ferries build high-speed aluminium trimarans, catamarans, and monohulls.

2. BACKGROUND

2.1 FATIGUE IN HIGH-SPEED LIGHT CRAFT

Fatigue is caused by fluctuating loads or stresses. In shipping, fatigue can arise from propulsion induced loads and vibrations, varying cargo-loading conditions or loads in a seaway such as wave-induced pressure and ship motions generating cyclic stresses (Fricke, 2017). Whilst fatigue is an issue in both steel and aluminium alloy ships, knowledge regarding fatigue in aluminium vessels is lacking compared to steel counterparts (Soliman, Barone and Frangopol, 2015).

Some of the complications in assessing aluminium alloy structures for fatigue arise from the material properties. 5000 series high magnesium aluminium alloys are typically used in a marine environment due to their resistance to corrosion and welding characteristics (Davis, 2001). Saltwater corrosion and welding techniques can significantly affect the fatigue strength of these materials (Mcdowell, 1977), complicating the analysis process. Compared with steel, aluminium alloys are less resistant to crack initiation resulting from welding defects (North *et al.*, 2000). Aluminium alloy ships also tend to feature weight-optimised scantlings and complex structural details, and are operated at speeds and in sea states where highly transient loads (such as slamming) are more likely to occur (Magoga, 2019; Lavroff *et al.*, 2017).

Det Norske Veritas (DNV) are the classification society responsible for classifying the Incat Tasmania WPCs. The Rules for Classification of High Speed and Light Craft (DNV GL, 2020) outline the rules and guidance pertaining to fatigue analysis in this vessel type. It states that the fatigue life for the craft is sufficient if rule design load levels, and appropriate allowable stresses are used. Critical areas which require fatigue analysis are listed, however the guidance offered on how to perform this is limited.

2.2 FATIGUE IN WAVE PIERCING CATAMARANS

Fatigue in WPCs has been studied previously using both measured and estimated stress histories. Thomas *et al.* (2006) used full scale measured data from Incat Hull 042 acquired during the delivery voyage and normal operations to analyse the effects of slamming on fatigue life and to quantify its effects. The research concluded that increasing occurrence of slam events and significant wave height both correlated with a decrease in the fatigue life of the ship structure in WPCs. It was also suggested that whipping behaviour (the hydro-elastic response to slamming), particularly the decay coefficient, may also strongly influence the fatigue life. As such the findings of this research suggest that WPCs may need a more specific approach to fatigue due to their unique hull forms and structural configurations.

Yang et al. (2014) used peak stresses derived from hydrodynamic simulations, Finite Element Analysis (FEA), and stress response transfer functions for a variety of sea states to calculate the predicted fatigue life for a generic WPC at typical stress hotspots. Rayleigh distributions were fitted to each short-term sea state and wave heading. These were then combined into a long term stress distribution using a closed-form solution in accordance with DNV GL (2015). The Rayleigh distribution is a special form of the Weibull distribution where the shape factor is set to two (Rinne, 2008). This method differs from the method outlined in this paper as it considers both multiple headings and multiple sea states (short-term wave loadings) and is thus computationally more intensive. The results of this analysis showed that multiple analysed locations did not meet the design fatigue life of 20 years, with the lowest calculated as 12.1 years. This paper was however limited as the generic WPC considered was a hypothetical vessel which was never constructed, and it used simulated data without validation of the resulting stress time histories. Furthermore, the use of potential flow methods may be inaccurate when used to calculate stress time histories for wave piercing catamarans (McVicar *et al.*, 2018). These results are also not reflective of the in-service performance of these vessels.

Soliman, Barone and Frangopol (2015) reported on a detailed analysis of fatigue in various sea states and wave headings using full scale data from sea trials measured on a 98m WPC designed by Revolution Design and built by Incat. This was achieved by relating various parameters such as sea state, heading and deployment state of the T-foil with the reliability factor (β) over the lifetime of the vessel. β is related to the probability of failure when using the Cumulative Density Function (CDF) of the standardised normal distribution (European Committee for Standardization, 2009). The results of this analysis showed that fatigue accumulation is highly complex with sea state, heading, speed and T-foil deployment state all being significant influencing factors. While this analysis would have to be combined with long term usage statistics to arrive at an accurate fatigue prediction, it offers a unique insight into which environments and vessel configurations result in comparatively high fatigue accumulation.

3. RATIONALE

DNV does not require fatigue analysis when rule loads and stresses are used in design, however there are instances when fatigue analysis is required, such as when designers develop novel hull-forms. Due to the nature of

WPC hull-forms, potential flow methods are unable to capture the re-entrant flow fields present during bow entry of a WPC. Accordingly, most seakeeping simulation work in literature uses a finite volume method to discretise either the RANS or Euler Equations (McVicar *et al.*, 2018). Such methods are significantly more computationally intensive that potential flow methods and long term runs over large numbers of conditions as would be required for direct fatigue assessment are impractical. In these circumstances, DNV provide guidance on how to perform fatigue analysis using a simplified approach, relying on only minimal use of CFD, to develop stress spectra. Such a simplified approach will generally be conservative, which may lead to oversizing of scantlings, or the requirement for resource intensive manufacturing processes (such as particular welding methods) to meet the fatigue design life.

The primary goal of this research is to compare fatigue damage estimates calculated from stress spectra produced with a simplified approach, to calculations performed on stress spectra derived from measured data from a WPC undergoing normal operations. A secondary goal is to quantify the impact of the unique design and operational profile of WPCs on the shape of the stress spectra, and the ability to fit a probability distribution. An Incat Tasmania ferry (Hull 091) fitted with a hull monitoring system was used as the basis for the analysis (Figure 1). Data was collected during the delivery voyage and regular ferry duties in the Canary Islands.

4. DATA ACQUISITION AND ANALYSIS

Incat Hull 091 (*Volcán de Tagoro*) was launched in July 2019. The University of Tasmania, in collaboration with Revolution Design and Softwire Systems, instrumented this vessel with an array of sensors to record data on-board and upload remotely to cloud storage for processing or retrieval at the end of each voyage. Approximately 1800 hours of ship usage data was included in this analysis collected between the 16th of July 2019 and the 31st of January 2020.

4.1 PHYSICAL LOCATION OF SENSORS

The focus of this paper will be on a single strain gauge located on the port side keel of the ferry at void 6 shown in Figure 1 (highlighted). This is a linear strain gauge positioned to predominantly measure the longitudinal bending response of the vessel. This strain gauge was selected as it is primarily influenced by global wave loading. Out of the three keel strain gauges it is also closest to the midship and therefore the highest stress values are anticipated offering the best signal to noise ratio.

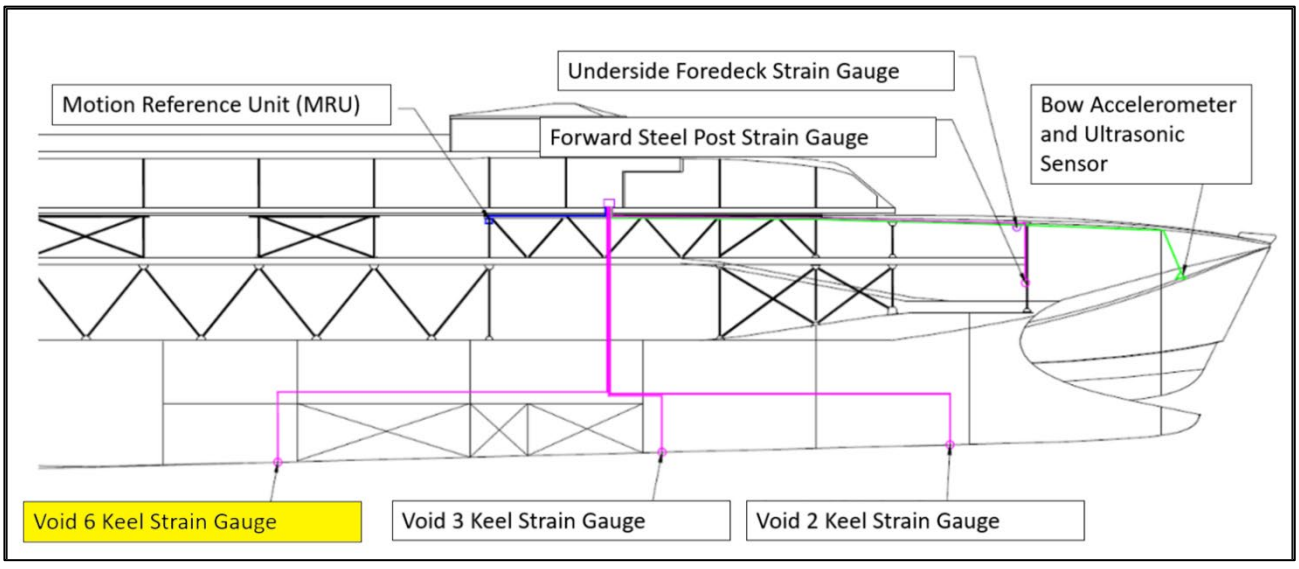

Figure 1: Profile view of forward part of INCAT Hull 091 (Volcán de Tagoro), 111m, deployed between Las Palmas and Tenerife in the Canary Islands (2019/2020) showing locations of onboard sensors.

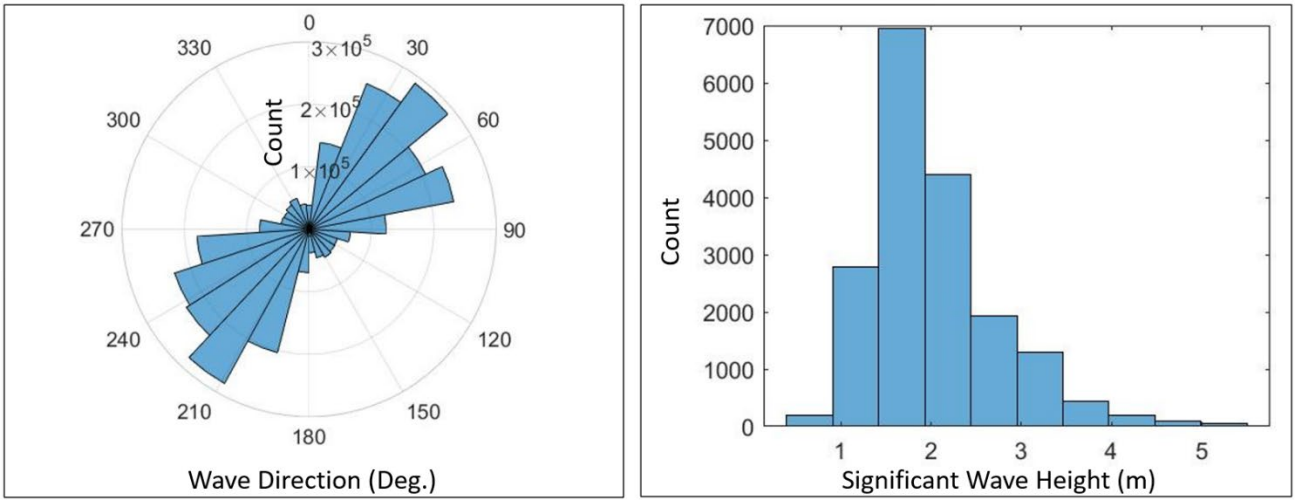

Figure 2: Swell direction relative to ship (left) and distribution of encountered significant wave heights (right). Significant wave height counted once per 5 minute segment, swell direction relative to ship counted with each recorded true heading update (approximately one count per 1.76s).

4.2 MEASURED ENVIRONMENT

The vessel operates on a route between Las Palmas and Tenerife in the Canary Islands, West Africa. Swell direction (relative to the bow) and significant wave height data is shown in Figure 2 for regular ferry duties in this location. These data sets were produced using GPS position and direction recorded on the vessel, cross referenced with historical wave data (Copernicus Marine Service, 2020). The swell direction in the Canary Islands was northerly biased resulting in the vessel being subjected to primarily bow seas and stern quartering seas when considering both route directions. Data was also recorded on the delivery voyage between Hobart, Australia, and the Canary Islands.

4.3 DATA FILTERING AND CONDITIONING

Strain signals were recorded in consecutive 5-minute sets, with data processing steps applied to each set independently. Filtering followed recommendations in DNV GL (2018) for hull monitoring systems with consideration for the dynamic response of the ship. A 0.01 Hz high-pass filter with 60 dB stopband attenuation and steepness of 0.95 followed by a 5 Hz low-pass filter with 60 dB stopband attenuation and steepness of 0.95 were applied to each 5-minute segment. The low-pass filter was selected to be a higher than the primary whipping mode, which is estimated in Hull 091 to be 2.44Hz based on a similar sized catamaran (Lavroff *et al.* 2013).

Although not included in the DNV guidelines, linear detrending was also applied to the data before filtering to compensate for Direct Current (DC) drift and to avoid edge effects.

An example post-filter time-waveform showing the highest peak stress event during the recording period is shown in Figure 3.

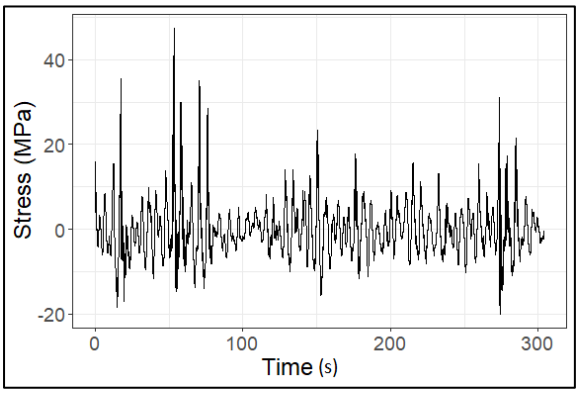

Figure 3: Example time waveform showing stress calculated from a strain recording made of the port void 6 strain gauge

4.4 FATIGUE ESTIMATION

The concept of linear cumulative damage in fatigue was originally proposed by Palmgren (1924) and popularised by Miner (1945) as a practical tool for estimating the remaining life of a component under cyclical stress. This relationship is shown in Equation 1, where the likelihood of fatigue cracking reaches unacceptable levels when $D = 1.0$. N is the output of an S-N Curve, that estimates the total number of cycles at a given stress-cycle range a material/geometry can tolerate without failure. This curve is determined experimentally, and N is often calculated as the average number of cycles at a given amplitude that a material/geometry combination has survived plus two standard deviations. The parameter j is the number of different amplitude levels (or bins) included in the analysis and typically corresponds to the number of bins in a stress spectrum.

$$D = \sum_{i=1}^{j} \frac{n_i}{N_i} \quad (1)$$

The selection of the S-N Curve influences the overall sensitivity of the resulting fatigue life to differences in stress-range. Therefore, for a comparative analysis, it is essential to select a curve that is common within HSLC. An S-N curve (curve II) from DNV (1997), shown in tabulated form in Table 1, was chosen as a typical S-N Curve. This S-N curve is representative of a welded joint in an area not exposed to saltwater. According to DNV (1997), it applies to all wrought standard aluminium alloys and temper conditions used for the design of aluminium alloy hull structures and applies to cruciform joins, termination of stiffeners on plates, and butt welds.

Table 1: S-N curve II for welded joints (DNV, 1997)

Region A		Region B	
$N \leq 5 \cdot 10^6$		$N > 5 \cdot 10^6$	
log a	m	log a	m
13.82	4.32	17.12	6.32

The S-N curve is generally implemented in the form of Equation 2 (DNV, 1997) where $\Delta\sigma$ is the stress-range in MPa (taken in this analysis as the average stress for the spectrum bin). Rearranging the equation to find N results in Equation 3. For simplicity to find N_i in Equation 1, the maximum value of N produced from either Region A or Region B (Table 1) using Equation 3 was used.

$$\log_{10} N = \log_{10} a - m \log_{10} \Delta\sigma \quad (2)$$

$$N = a \cdot \Delta\sigma^{-m} \quad (3)$$

To account for the difference in stress between the nominal stress (those derived from beam element models, or measured at a strain gauge located away from the weld detail) and the notch stress, a stress concentration factor must be used, typically referred to as K (Equation 4) (DNV, 1997).

$$K = \frac{\sigma_{notch}}{\sigma_{nominal}} \quad (4)$$

The stress concentration factor (K) must relate to a specific geometry and weld configuration, the precise details of which are not always known. As such a range of K factors were considered in the analysis where possible. Additionally, where such details were unknown, a value of 3 was used, which was the highest value across geometries included in (DNV, 1997).

4.5 RAINFLOW CYCLE COUNTING

To estimate the number of cycles for each stress range (n_i) the signal must first be processed from a time-waveform into a stress histogram. The rainflow algorithm proposed by Matsuishi and Endo (1968) solves part of this problem by reducing a time-waveform stress-history into a set of stress reversals. A comprehensive description of how rainflow counting is used in fatigue analysis is presented by Lalanne (2014), along with some alternative cycle counting techniques. For this work an existing MATLAB function was used to implement this algorithm (Nieslony, 2020) which is in accordance with ASTM International (2017).

4.6 CREATING THE STRESS SPECTRA

To form a stress histogram or stress spectra from the output of a rainflow counting algorithm two parameters were specified:

- The maximum expected stress range ($\Delta\sigma_0$) for the location of interest – this forms the stress value for the highest bin in the stress histogram
- The number of bins (N_{bins})

The maximum expected stress range ($\Delta\sigma_0$) was supplied by Revolution Design who used quasi-static FEA to determine the design loads at the location of interest (strain gauge location) during a maximum stress event in sag (σ_0). The load case considered was head seas under slamming conditions. This result was multiplied by the ratio between the full stress range and the maximum stress event in sag (R_{range}) to obtain the predicted maximum stress range. The design loads were scaled from hydrodynamic calculations performed by DNV on a similar vessel using their WASIM solver (DNV GL, no date) .

$$R_{range} = \left(\frac{\Delta\sigma_0}{\sigma_0}\right) \quad (5)$$

$$E = \frac{\Delta\sigma_0}{\Delta\varepsilon_0} \quad (6)$$

$$\Delta\varepsilon_0 = \frac{\sigma_0}{E} \cdot R_{range} \quad (7)$$

The values provided by Revolution Design were 88.8 MPa for σ_0 and 1.625 for R_{range} and the value for the stress range ($\Delta\sigma_0$) was calculated as 144 MPa. As the recorded data was in strain the magnitude of the highest bin was calculated using Equation 6, resulting in Equation 7 which incorporates the Young's modulus (E) to arrive at the maximum expected strain range ($\Delta\varepsilon_0$). The material was assumed to be aluminium alloy 5383 with a Young's modulus of 72 GPa. The number of bins was selected as 100 in exceedance of the DNV recommendations which suggest greater than 20 bins (DNV GL, 2018).

.4.7 RANKED CYCLE REMOVAL

In preliminary analysis a significant portion of the cycle counts were attributed to the lowest magnitude bin, even when a high number of bins was selected. This was found to cause skewing of the fitment of a Weibull curve even though stress cycles of this magnitude have a negligible effect on fatigue, even with high counts. To solve this, for each 5-minute time history sample, stress cycles were ordered from the most severe to the least severe and the number of ordered stress cycles retained was set to a constant as calculated using Equation 8 (where T_z is the assumed average ship response period, and $t_{section}$ is the record length of the analysed section of data in seconds).

$$N_{cycles} = \frac{1}{T_z} \cdot t_{section} \tag{8}$$

The average ship response period was approximated as the natural heave period of the vessel (T_z). A similar estimate is used to calculate the number of cycles for the lifetime fatigue calculations in DNV (1997). While the number of retained cycles is somewhat arbitrary, using Equation 8 ensures that the number of cycles encountered for a given number of operational hours is the same as the DNV method. This makes comparisons and extrapolation simpler.

Revolution Design supplied the measured heave frequency of a similar vessel as 0.28 Hz and the expected time at sea as 4500 hours per year. To account for the difference and for simplicity the heave frequency was assumed to be 0.25 Hz, meaning T_z is equal to 4s. This results in an expected number of cycles for the life of the vessel as 8.1×10^7 cycles and 75 cycles for each 5-minute time history. Fatigue life calculations using stress-spectra with and without ranked cycle removal did not vary significantly. Comparison between the spectra with and without ranked cycle removal showed a percentage error of 0.024% when fatigue life was calculated with a *K* factor of 3, however the Weibull fit improved drastically. This method is similar to that used in Bai et al. (2018) to achieve a similar result.

4.8 PROBABILITY DISTRIBUTION SELECTION AND FITMENT

The approximation of probability density functions (PDFs) to stress histograms is common in marine industry fatigue estimation (American Bureau of Shipping, 2016; Bai and Jin, 2016). Options for probability density functions that can be used in this context include linear, Weibull, Gaussian and exponential (Magoga *et al.*, 2016). For this paper, a 2 parameter Weibull function was selected as it is the distribution used in DNV GL (2015).

The selection of a function is not the only factor that has to be considered. Prior to fitting the function, decisions must be made on how to select and process the independent variable. Magoga *et al.* (2016) used various PDFs to estimate the stress range for a particular number of cycles. One of these equations is a variant of the Weibull function shown in Equation 9. This equation has three parameters (one shape factor X and two scale parameters λ and a_2) and sets the independent variable as the logarithm of the number of cycles in a stress histogram (n_i) with the output as the expected stress range. This approach leads to non-physical results in the high-stress region of the spectrum, which means that extrapolation is not possible using the Weibull distribution directly.

$$\Delta\sigma(n_i) = a_2 \cdot \lambda \cdot \mathrm{X} \cdot \log(n_i)^{\mathrm{X}-1} \cdot e^{(-\lambda \cdot \log(n_i))} \tag{9}$$

Munse (1981) sets the normalised stress cycle range as the independent variable and calculates the number of cycles for each stress range using percentages obtained from the PDF. Variations of this method (including the method in DNV GL (2015) uses integrals of the PDF created using the Weibull function to recreate the number of cycles in each bin. This is seemingly a more traditional way to use the Weibull distribution, more consistent with Weibull's original application to the risk of rupture of rods made of stearic acid and plaster-of-Paris (Rinne, 2008). A two-parameter Weibull function was used by Munse (1981) to estimate the probability density function as a function of stress, as shown in Equation 10, where k is the shape parameter and w is the characteristic value of $\Delta\sigma_x$, otherwise known as the scale factor.

$$f_s(\Delta\sigma_i) = \frac{k}{w}\left(\frac{\Delta\sigma_i}{w}\right)^{k-1} \exp\left(-\frac{\Delta\sigma_i}{w}^{k}\right) \tag{10}$$

A variety of methods exist to fit the required parameters, including but not limited to least squares and linear approaches, maximum likelihood approaches, methods of moments, and Bayesian (Rinne, 2008). Due to its simplicity and closed-form nature, the method outlined by Munse (1981) was used in this paper. To estimate the first parameter, k the coefficient of variation is first calculated using Equation 11, where δ is the coefficient of variation, SD is the standard deviation, and μ_S is the mean stress level of the measured distribution. Munse (1981) used the mean stress and standard deviation of a Weibull distribution to calculate the coefficient of variation for a variety of shape factors, which he presented in table form. By aligning the coefficient of variation of the measured spectrum (Equation 11) with a coefficient of variation from the closest Weibull distribution, using Munse's pre-solved table, the shape factor can be estimated. The values tabulated by Munse (1981) were interpolated to allow for higher precision. The centre point between the upper and lower bound of each bin of the measured distribution was used. Fitment was performed on pre-log transformed data.

$$\delta = \frac{SD}{\mu_S} \quad (11)$$

The final parameter, w (the characteristic value of $\Delta\sigma_x$, or scale factor), can then be estimated using Equation 12 where Γ is the Gamma function.

$$w = \frac{\mu_S}{\Gamma(1+\frac{1}{k})} \quad (12)$$

This method offers a simple way to estimate the shape factor that does not rely on numerical methods. This has advantages in developing simple tools such as spreadsheets, or onboard processing algorithms where complex fitting functions are not always available. Furthermore, this method is more easily applied to data which has been reduced to a stress spectrum (or histogram) as it only requires the mean stress and standard deviation. Numerical methods often require stored individual cycles to perform the fitment, however it is possible to reproduce these from a histogram, with a reduction in precision.

To compare this method to a numerical method, a maximum likelihood estimation was performed in Matlab and the coefficient of determination (R^2) was calculated for each. Weibull parameters and resulting R^2 values for both fitment methods are shown in Table 2. This shows negligible differences in R^2 values between the two methods.

4.9 COMBINED WEIBULL FITMENT BASED ON SLAM DETECTION

Preliminary analysis showed that the stress spectra created from the measured data diverged from the Weibull fitted function at higher stress terms, as shown in Figure 5 (bottom left) of the results. While fitted low-stress terms appear visually to be a good fit to the Weibull distribution, higher stress terms diverge markedly which is a phenomenon not typically seen when the data originates from a conventional ship (Munse, 1981). Non-linearity in Weibull fitment is discussed in Mclinn (2010) which highlights various causes for poor Weibull fitment in the context of reliability/failure prediction. While many of these causes were non-analogous to wave loadings, non-linearity caused by mixed failure modes may be comparable to varied loading types in HSLC. Due to slamming or bow entry events the origin of the stress cycles on the hull cannot be fully attributed to typical wave loadings and this may be the cause of the divergence. As such, a filter was proposed to separate time-waveforms that contain significant slam events to see if a better fit could be achieved by combining spectra fitted to the two separate categories of wave loadings.

Detection of slams has been performed on WPCs and HSLC more generally using a variety of methods. Magoga *et al.* (2017) concluded that whipping stress rate was the most successful criterion for slam identification which was originally proposed in Thomas *et al.* (2003). This paper used a stress-rate of 5 MPa/s for slam identification, however also suggested the boundary between a slam occurring and not occurring was not strictly defined.

As such, an optimised threshold to efficiently identify slams for the purpose of developing a second Weibull fit was derived experimentally. To arrive on an optimised slam criterion a Weibull fit was applied to the histograms formed by time-histories from above and below a range of stress-rate criterion. A resulting fit was formed by summing those two spectra. R^2 and percentage error for fatigue life compared with the measured spectra (with an assumed K factor of 3) were calculated for each. The results are shown in Table 4.

One issue with assessing the quality of a parameter fit with R^2 is that it does not consider exponential effects applied to the spectra, such as those used in the calculation of fatigue life. Furthermore, the differences in R^2 were insignificant between thresholds. For this reason, the fatigue calculation was used to select an optimal threshold which resulted in a stress rate of 54 MPa/s. The final spectrum was created by summing the number of cycles from each sub-fitment and is referred to hereafter as the combined Weibull distribution.

4.10 PRESCRIBED STRESS SPECTRA (DNV METHOD)

A simplified long-term stress distribution is presented in DNV GL (2015). This method is based on the Weibull distribution, except it is described in terms of the exceedance function, defined in Equation 13 and Equation 14 in terms of the Cumulative Density Function (CDF), resulting in Equation 15. Using this equation

Table 2: Comparison of Weibull parameter fitment methods

	Shape Parameter (k)	Scale Parameter (w)	R^2
Tabular Method	1.15	3.56	0.999
Maximum Likelihood	1.14	3.48	0.998

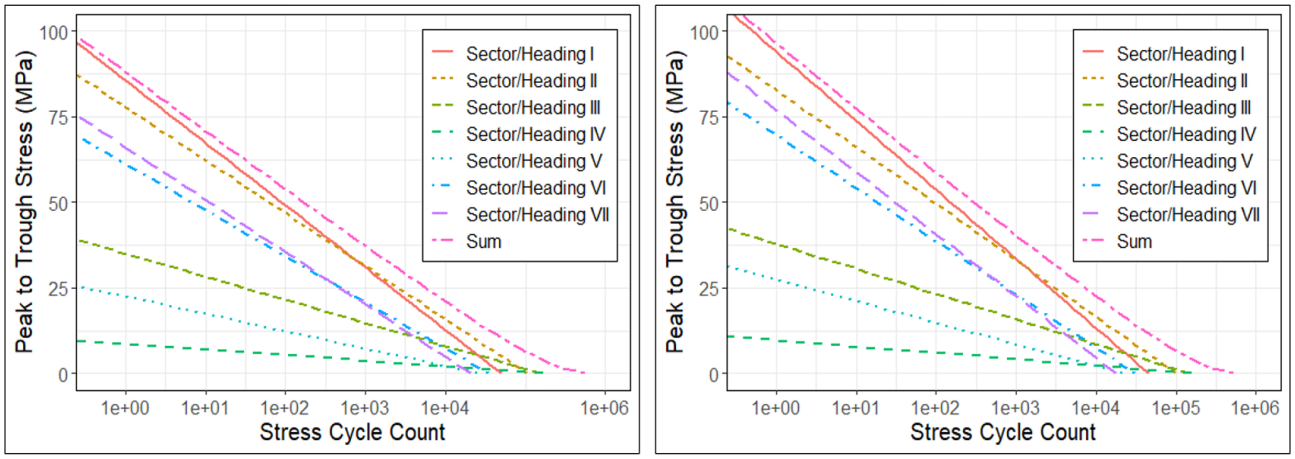

Figure 4: Spectra derived using simplified DNV method with maximum expected stress event set to happen once per life of vessel (left) and with maximum stress event set to happen once per heading (right).

allows for the maximum expected stress to be prescribed a likelihood of occurrence of 1 (i.e., $Q(\Delta\sigma_0) = 1/n_0$), using the scale factor shown in Equation 16.

$$Q(\Delta\sigma_i) = Pr[\Delta\sigma > \Delta\sigma_i] = 1 - F(\Delta\sigma_x) \quad (13)$$

$$F(\Delta\sigma_i) = CDF = 1 - e^{-\left(\frac{\Delta\sigma_i}{k}\right)^k} \quad (14)$$

$$Q(\Delta\sigma_i) = e^{-\left(\frac{\Delta\sigma_i}{w}\right)^k} \quad (15)$$

$$w = \frac{\Delta\sigma_0}{(\ln n_0)^{\frac{1}{k}}} \quad (16)$$

For this analysis, the maximum expected stress ($\Delta\sigma_0$) was also set using the FEA results outlined in Section 4.6 so that the spectra would be comparable.

DNV (1997) also prescribes a directional distribution of waves, which allows for separate Weibull distributions to be formulated for different headings, based on reduced maximum stresses. Revolution Design supplied reduction factors for mean headings in 30º increments, which reduces the maximum stress used to calculate fatigue in each sector. DNV (1997) provides an estimate for how many cycles can be attributed to a particular heading as shown in Table 3.

Incorporating multiple headings introduces an ambiguity in the calculation method through the selection of n_0, which details the number of cycles associated with the maximum stress event $\Delta\sigma_0$. The maximum stress event or design stress is set to occur once in the lifetime of the vessel however by sectoring the wave headings only 17% of the response cycles are allocated to conditions which are assumed to prompt a design limit event (head seas). Reducing n_0 to the cycle count associated with each wave heading means the vessel undergoes a design limit event once in each heading (although aside from head seas, the maximum stress will be reduced by the factors shown in Table 3.

Reducing the number of cycles associated with the peak event (n_0) has a flow-on effect for the entire distribution and yields a more conservative result in fatigue calculations. While this is the only way to ensure one maximum stress event is included in the analysis it does not make physical sense, as if the number of considered wave headings (which is arbitrary) is increased it also increases the number of maximum stress events. Whilst Revolution Design adopt this conservative approach, both methods are included here for comparison.

Figure 4 shows the underlying spectra and final summed spectrum for each method. The two methods used in this figure are referred to in the results as “DNV by Heading” (whereby n_0 is associated with the cycles encountered in each heading, meaning one design limit event will occur in each sector, or seven times in total) and “DNV by Life” (whereby n_0 is associated with the cycles encountered in the life of the vessel, meaning one design limit event will occur during the life of the vessel).

Table 3: Ratio of the number of stress cycles apportioned for each sector DNV (1997)

Sector	Mean Heading	N_{ih}/N_{total}
I	0º	0.17
II	+/-30º	0.31
III	+/-60º	0.23
IV	+/-90º	0.11
V	+/-120º	0.03
VI	+/-150º	0.09
VII	180º	0.06

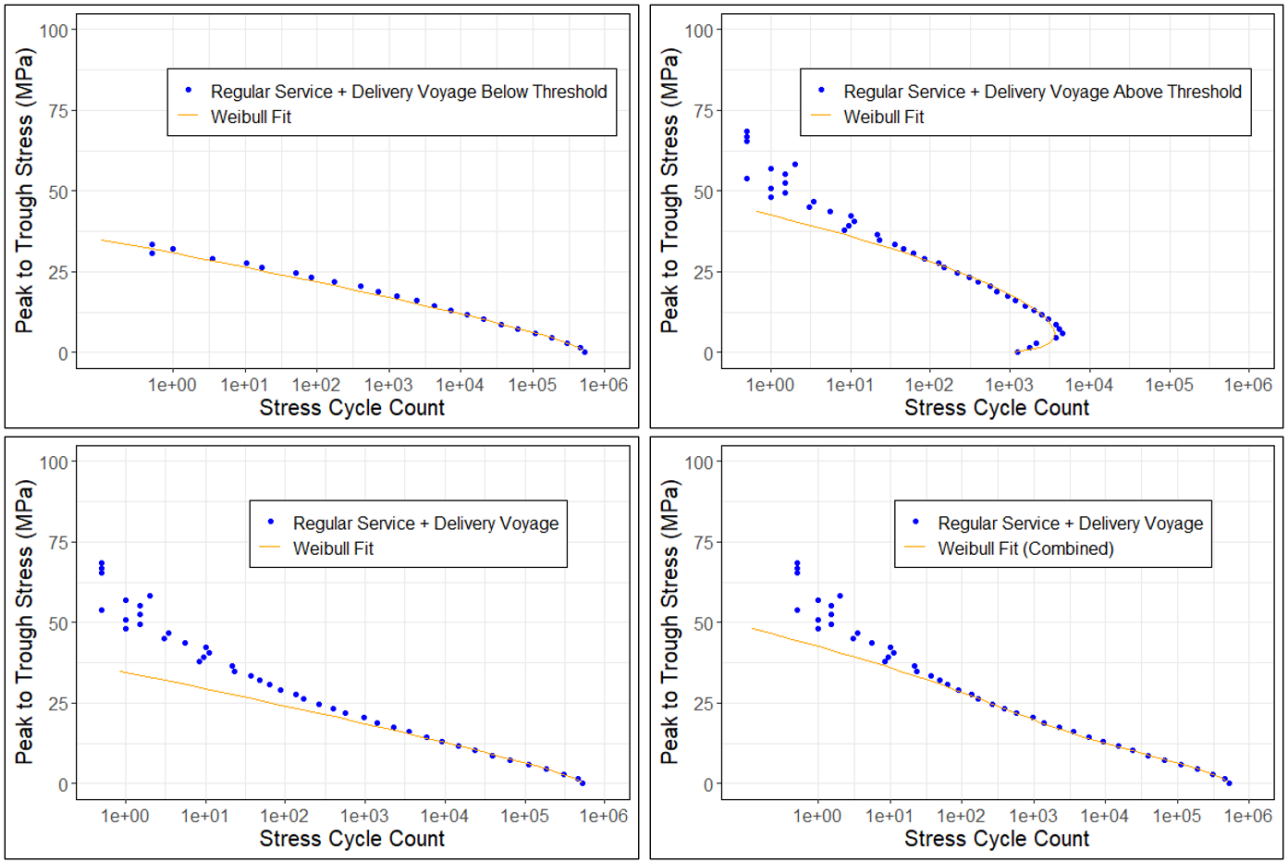

Figure 5: Stress spectra and Weibull fit from data below (top-left) and above (top-right) the stress-rate threshold. Stress spectra and weibull fit made using traditional fitment methods (bottom-left) and using a combined Weibull fit (bottom-right)

4.11 RECOVERING THE STRESS SPECTRA FROM WEIBULL PARAMETERS

The exceedance function was used to estimate the number of stress events for each bin (n_i), based on the total number of stress events (n_l). This function does not require integration to determine the correct probability for each bin, which makes re-forming spectra simpler than if a probability density function is used directly. To determine the discrete number of events for each bin (rather than the number of events which exceed the stress level for each bin) Equation 17 is used for the maximum stress event, and Equation 18 is used for all lower terms.

$$n_0 = n_l.Q(\Delta\sigma_0) \tag{17}$$

$$n_i(\Delta\sigma_i) = n_l.(Q(\Delta\sigma_i) - Q(\Delta\sigma_{i+1})) \tag{18}$$

This method was used to form the stress spectra from the DNV prescribed method as well as to reform spectra using Weibull distribution approximations. Due to these equations being based on exceedance the left-hand side of each bin was used for the calculation.

5. RESULTS AND DISCUSSION

5.1 COMPARISON OF STRESS SPECTRA

The stress spectra formulated using the DNV methods alongside spectra formed using measured data

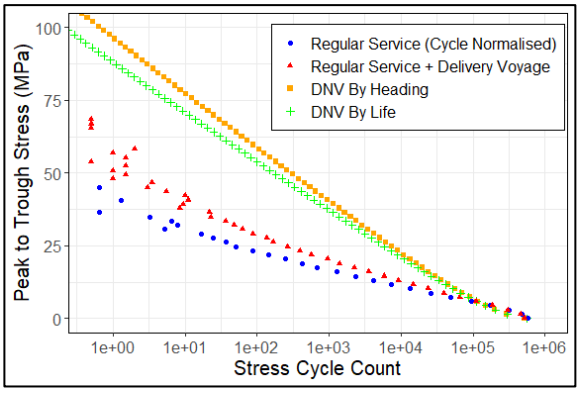

Figure 6: Comparison of derived and measured stress spectra

directly are shown in Figure 6. The total number of cycles in the regular service spectra was normalised to equal the total number of cycles experienced by the vessel during the regular service plus the delivery voyage (1.75×10^6 cycles). Similarly, the number of cycles analysed in the DNV spectra was also set to this value. This comparison shows that the simplified DNV method does not reproduce the shape, nor the scale of stress spectra constructed from measured results.

The deviation from measured results can largely be attributed to the use of the maximum design stress range ($\Delta\sigma_0$) to derive the scale parameter in the Weibull distribution (i.e., Equation 16). Using this equation produces a distribution that contains higher counts for larger magnitude stress cycles than what is seen in measured data.

Another source of conservatism is the introduction of the R_{range} of 1.625. This value is determined from an assumed ratio of sagging to hogging of 1.6, supplied by Revolution Design and accepted by DNV GL. This ratio may not be representative of a vessel undergoing slamming. For example, the signal shown in Figure 3 (which is the highest stress peak during the measured period) has a positive stress of 47.3 MPa but the worst-case stress range was identified by the rainflow counting algorithm as a half count with magnitude 67.7 MPa. So R_{range} from the example taken from the measured data is 1.43.

5.2 WEIBULL FIT COMPARISON

The spectra formed from below and above the stress rate threshold and the single Weibull fit (performed on unfiltered data) are compared with the combined Weibull fit in Figure 5. Results including the R^2 and fatigue estimates for the standard Weibull fit and the combined Weibull fit with stress rate filtering are shown in Table 4. This shows that the error is reduced by approximately half when the improved fit is used with a stress rate criterion of 54 MPa/s.

A residual error of 19% still exists, which at first appears to be due to the Weibull fit not accommodating the scattered higher stress terms, however by plotting the error accumulation in fatigue terms against the Peak to Trough Stress (shown in Figure 7) it can be seen that much of the error occurs at lower stress values, and from the section of the spectrum that was largely dictated by wave loadings that fell below the stress rate threshold.

Comparing Figure 7 with Figure 5 (bottom right) highlights that even if a fit is accurate visually with a high R^2, small errors can compound once the fatigue calculations are made. Similar errors may exist for non-HSLC fits and may be a limitation of the Weibull fit itself. For example, long term Weibull fits were used in Bai *et al.* (2018) to describe the fatigue accumulation in fish cages, which found that the fatigue life estimate of the Weibull fit was approximately 50% that of a fatigue life calculated using measured data. In this case the primary difference is that Bai *et al.* (2018) yielded conservative results. This suggests that the accuracy of the fit produced in the results (19%) may be within acceptable limits, but due to its under-conservatism may require a safety factor to be applied to the final fatigue life estimate. The way in which the ranked cycle removal was conducted may also contribute to the accuracy of the Weibull fit and further research may uncover a more suitable strategy to remove insignificant stress terms prior to Weibull fitment.

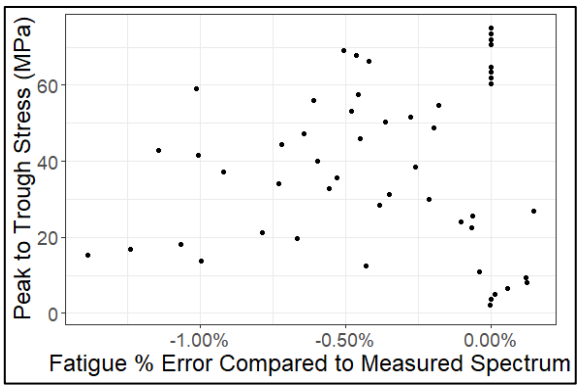

Figure 7: Relative contribution to fatigue error for each stress bin

A comparison of Weibull parameters (inclusive of the delivery voyage) is shown in Table 5. Also shown is the percentage error compared with calculations made directly with the measured spectra when predicting fatigue with a K factor of 3. Due to the DNV method containing a multitude of scale factors, depending on heading, the

Table 4: Optimisation of stress-rate criterion threshold for creation of combined Weibull spectrum

Stress-Rate criterion MPa/s	Percentage of data above threshold	R^2 of combined spectrum	Weibull fatigue life percentage error
N/A	0	0.998	41
5	79.6	0.995	44
18	29.2	0.999	33
36	5.53	0.999	19
54	2.02	0.999	19
72	1.11	0.999	21
108	0.7	0.999	23

Table 5: Comparison of Weibull fits and percentage error for fatigue calculations

Spectrum	Shape Parameter (k)	Scale Parameter (w)	Percentage Error
DNV By Heading	1	26.0	+3125
DNV By Life	1	23.5	+2019
Weibull	1.15	3.56	-43
Improved Weibull	1.2/1.68	3.46/11.06	-20

Weibull parameters for the dominant heading is shown (head seas) which dictated approximately 45% of the fatigue accumulation in both cases. The two parameters listed under the dual-fit Weibull distribution are for the spectra fitted with wave loadings below and above the stress-rate threshold (consecutively).

5.3 FATIGUE ESTIMATION

Results for fatigue accumulation (D) are shown for a variety of K factors in Table 6. These results also show fatigue estimates using both the standard and combined-fit Weibull distribution methods. To highlight the stress levels that were most responsible for fatigue accumulation, a graph showing the fatigue damage associated with each stress cycle bin for each spectrum is shown in Figure 8 for measured and derived results. The regular service results are normalised by cycle count, with regular service plus delivery voyage as the baseline. Similarly, the DNV method was based on the number of cycles associated with the regular service plus delivery voyage. These results show that the DNV method does not compare accurately to the measured results (from the standpoint of fatigue) either in shape or magnitude for either regular service in the Canary Islands, even if the delivery voyage from Hobart Tasmania to the Canary Islands is included.

The results in Table 6 show that the Weibull fits applied to the measured data are far more accurate than those generated using the DNV method in terms of the magnitude of error, however they both provide under-conservative estimates. Accuracy may also reduce further with extrapolation. Furthermore, the data collection is limited to one vessel, and largely one ferry route which was known to have a bias in terms of the average wave heading (Figure 2). As such it would not be appropriate to substitute these wave loadings in design without further research which provided a spectrum that accounted for the full range of conditions this vessel type may encounter. In some cases, vessels may be operated on a specific route in which case a less conservative spectrum calculated using route specific analysis may be appropriate.

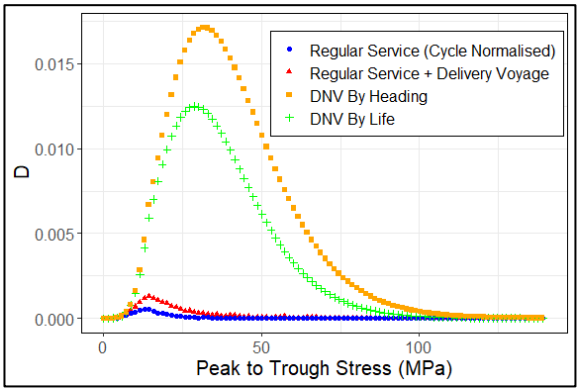

Figure 8: Fatigue damage vs peak to trough stress for derived and measured stress spectra

Fatigue assessment would not normally be required in the studied area of the ship under the DNV rules based on the allowable design stress levels. As such it would be expected that this region should pass any fatigue assessment with a significant margin. Given the results of this paper it can be concluded that the fatigue failures indicated by the application of the simplified DNV method in this region (Table 6) is a "false failure" suggesting that this method likely contains a higher amount of conservatism than required. This is supported by the historical in-service performance of these vessels, as well as the in-service data gathered from Hull 091 which both suggest that the vessels are capable of meeting design fatigue life requirements.

Table 6: Comparisons of lifetime fatigue estimates (D = 1 predicts failure)

	D (life of vessel)		
Fatigue life calculation method	$K = 1$	$K = 2$	$K = 3$
DNV By Life	8.23E-02	2.46E+00	1.50E+01
DNV By Heading	1.37E-01	3.80E+00	2.28E+01
Extrapolated Measured Data (Regular Service)	3.45E-04	2.34E-02	2.19E-01
Extrapolated Measured Data (Delivery Voyage Included)	1.89E-03	9.10E-02	7.08E-01
Weibull (Regular Service)	1.45E-04	1.15E-02	1.32E-01
Weibull (Delivery Voyage Included)	5.46E-04	4.10E-02	4.02E-01
Improved Weibull (Regular Service)	2.39E-04	1.76E-02	1.73E-01
Improved Weibull (Delivery Voyage Included)	1.13E-03	6.97E-02	5.67E-01

6. CONCLUSIONS

The results show that the spectra derived from classification society guidelines using a simplified approach estimate a higher amount of fatigue damage compared with spectra derived from measured data. For an assumed *K* factor of 3 the DNV Method estimates fatigue at a rate 32.25 times greater than estimates produced with measured data. The study is however limited to one global location, with a known wave heading bias and the results may differ significantly for other operating environments.

A combined Weibull fit was proposed, that showed a reduction in error when calculating fatigue of approximately 50%, however the fatigue calculations relying on this fit were still under-conservative compared with calculations made directly with the measured spectra. Non-linearities compared with the Weibull fit may be attributable to the effects of slamming or bow entry, however other unknown effects may be present. Further research into appropriate fitment methods from stress spectra originating in HSLC is recommended.

This research highlights the importance of ensuring fatigue calculation methods that have been adapted from methods traditionally used on conventional ships are suitable for use on load-cycle analysis for WPCs and HSLC. The application of existing methodologies may have limitations particular to these vessel classes when simplified methods are used to derive stress spectra.

While the conservatism is substantial in this case, research that includes a wider range of vessels and environments would be required before changes to existing methodologies could be proposed. This paper does however highlight an area in class guidelines in which significant improvements may be possible, potentially leading to more efficient structural design, particularly when the vessel's specific operating environment is considered. Collection of full-scale data in the vessel investigated in this paper as well as other similar vessels is ongoing, and further systematic investigations are recommended to examine the relationship between fatigue damage accumulation, structural loads, slamming and operating conditions for WPCs. Calculating fatigue for a wider range of conditions may be possible through incorporating non-parametric and machine learning models as well as hind-cast or measured wave statistics.

7. ACKNOWLEDGEMENTS

This paper would not have been possible without the contribution made by industry partner Revolution Design, notably Tim Roberts and Gary Davidson. The authors also thank Keith Joiner (UNSW) and Michael Davis (UTAS) for their feedback and advice. This research was undertaken through the support of the Australian Research Council (ARC) grant number LP170100555.

8. REFERENCES

1. ABS (2016) *ABS Guide for Spectral-Based Fatigue Analysis for Vessels*. American Bureau of Shipping, Houston, USA.
2. ASTM International (2017) *ASTM E1049-85 Standard Practices for Cycle Counting in Fatigue Analysis*. ASTM International. Available at: https://www.astm.org/e1049-85r17.html.
3. BAI, X., ZHAO, Y., DONG, G. and BI, C. (2018) *Probabilistic analysis and fatigue life assessment of floating collar of fish cage due to random wave loads*, Applied Ocean Research, 81 (November 2017), doi:10.1016/j.apor.2018.09.018.
4. BAI, Y. and JIN, W.L. (2016) *Marine structural design*. Butterworth-Heinemann, Oxford, UK.
5. Copernicus Marine Service (2020) *Global Ocean Waves Analysis and Forecast*. Available at: https://resources.marine.copernicus.eu/?option=com_csw&view=details&product_id=GLOBAL_ANALYSIS_FORECAST_WAV_001_027.
6. DAVIS, J.R. (2001) *Aluminum and Aluminum Alloys*, in Alloying: Understanding the Basics. ASM International, Portland, USA.
7. DNV (1997) *DNV Report No 97-0152 Proposal for Classification Note: Fatigue Analysis of HSLC*. 97–0152.
8. DNV GL (2015) *DNVGL-CG-0129: Fatigue Assessment of Ship Structures.* Hovik, Norway.
9. DNV GL (2018) *Rules for Classification, Ships, Part 6 Additional class notations, Chapter 9 Survey arrangements*. Hovik, Norway.
10. DNV GL (2020) *Rules for Classification High speed and light craft, Part 3 Structures, equipment, Chapter 9, Direct calculation methods.* Hovik, Norway.
11. DNV GL (no date) *Linear and non-linear hydrodynamic analysis of vessels including forward speed - Wasim*. Available at: https://www.dnv.com/services/linear-and-non-linear-hydrodynamic-analysis-of-vessels-including-forward-speed-wasim-2413 (Accessed: 24 January 2022).
12. European Committee for Standardization (2009) *EN 1999-1-1:2007+A1 Eurocode 9: Design of aluminium structures - Part 1-1: General structural rules.* Brussels, Belgium.
13. FRICKE, W. (2017) *Fatigue and Fracture of Ship Structures*, Encyclopedia of Maritime and Offshore Engineering [Preprint]. doi:10.1002/9781118476406.emoe007.
14. INCAT (2019) *INCAT Hull 091*. Available at: https://incat.com.au/incat-vessels/091/ (Accessed: 18 January 2022).
15. LAVROFF, J., DAVIS, M.R., HOLLOWAY, D.S. and THOMAS, G. (2013) *Wave slamming loads on wave-piercer catamarans operating at high-speed determined by hydro-elastic*

segmented model experiments, Marine Structures, 33 (October 2013), doi:10.1016/j.marstruc.2013.05.001.

16. LAVROFF, J., DAVIS, M.R., HOLLOWAY, D.S., THOMAS, G.A. and McVICAR, J.J. (2017) *Wave impact loads on wave-piercing catamarans*, Ocean Engineering, 31 (February 2017), doi:10.1016/j.oceaneng.2016.11.015.
17. MAGOGA, T. (2019) *Development of a Structural Fatigue Life Assessment Framework for High-Performance Naval Ships*. UTAS Open Access Repository, Hobart, Australia.
18. MAGOGA, T., AKSU, S., CANNON, S., OJEDA, R. and THOMAS, G. (2016) *Comparison between fatigue life values calculated using standardised and measured stress spectra of a naval high speed light craft*, PRADS 2016 - Proceedings of the 13th International Symposium on Practical Design of Ships and Other Floating Structures [Preprint]. Copenhagen, Denmark. 4-8 September.
19. MAGOGA, T., AKSU, S., CANNON, S., OJEDA, R. and THOMAS, G. (2017) *Identification of slam events experienced by a high-speed craft*, Ocean Engineering, 140 (August 2017), doi:10.1016/j.oceaneng.2016.07.017.
20. MATSUISHI, M. AND ENDO, T. (1968) *Fatigue of metals subjected to varying stress*, The Japan Society of Mechanical Engineers [Preprint].
21. McDOWELL, K.A. (1977) *Fatigue behavior of aluminum alloy weldments in a marine environment.* Iowa State University.
22. McLINN, J.A. (2010) *Practical Weibull Analysis Techniques - Fifth Edition*. The Reliability Division of ASQ, MN, USA.
23. McVICAR, J., LAVROFF, J., DAVIS, M.R. and THOMAS, G. (2018) *Fluid–structure interaction simulation of slam-induced bending in large high-speed wave-piercing catamaran*, Journal of Fluids and Structures, 82 (October 2018), doi:10.1016/j.jfluidstructs.2018.06.009.
24. MINER, M.A. (1945) *Cumulative Fatigue Damage,* Journal of Applied Mechanic*s, 3*.
25. MUNSE, W.H. (1981) *Fatigue Criteria for Ship Structure Details*. Extreme Loads Response Symposium, The Society of Naval Architects and Engineers. Arlington, VA. 19-20 October.
26. NIESLONY, A. (2020) *Rainflow Counting Algorithm*, MATLAB Central File Exchange. Available at: https://au.mathworks.com/matlabcentral/fileexchange/3026-rainflow-counting-algorithm (Accessed: 13 August 2020).
27. NORTH, R.C., LIU, D.D., BYRNE, J., STREETER, B., CONNORS, T. and PEGG, D.N. (2000) *SSC-410 Fatigue of Aluminium Structural Weldments*. Ship Structure Committee(SNAME). Washington, VA.
28. PALMGREN, A. (1924) *Die Lebensdauer von Kugellagern,* Zeitschrift des Vereins Deutscher Ingenieure. Berlin, Germany.
29. RINNE, H. (2008) *The Weibull Distribution - A Handbook*. Chapman and Hall, London, UK.
30. SOLIMAN, M., BARONE, G. and FRANGOPOL, D.M. (2015) *Fatigue reliability and service life prediction of aluminum naval ship details based on monitoring data*, Structural Health Monitoring, 14 (December 2014), doi:10.1177/1475921714546059.
31. THOMAS, G., DAVIS, M.R., HOLLOWAY, D.S. and ROBERTS, T. (2006) *The effect of slamming and whipping on the fatigue life of a high-speed catamaran*, Australian Journal of Mechanical Engineering, 3 (2) (2006), doi:10.1080/14484846.2006.11464505.
32. THOMAS, G.A., DAVIS, M.R., HOLLOWAY, D.S., WATSON, N.L. and ROBERTS, T.J. (2003) *Slamming response of a large high-speed wave-piercer catamaran*, Marine Technology and SNAME News, 40 (02) (April 2003), doi:10.5957/mt1.2003.40.2.126.

